Journal of Marine Science and Technology

Volume 23 | Issue 2 Article 3

ROBUST BEARING ESTIMATION IN SHALLOW WATER USING VECTOR OPTIMIZATION

Hai-Yan Song
College of Information And Communication Engineering, Harbin Engineering University, Harbin, China. School of Electrical and Information Engineering, Heilongjiang Institute of Technology, Harbin, China.

Jie Shi
Acoustic Science and Technology Laboratory, Harbin Engineering University, Harbin, China. College of Underwater Acoustic Engineering, Harbin Engineering University, Harbin, China., shijie@hrbeu.edu.cn

Chang-Yi Yang
Department of Computer Science and Information Engineering, National Penghu University of Science and Technology, Magong, Taiwan, R.O.C.

Bo-Sheng Liu
College of Underwater Acoustic Engineering, Harbin Engineering University, Harbin, China.

Ming Diao
College of Information And Communication Engineering, Harbin Engineering University, Harbin, China.

ROBUST BEARING ESTIMATION IN SHALLOW WATER USING VECTOR OPTIMIZATION

Acknowledgements

This work was supported by the Specialized Research Fund for the Doctoral Program of Higher Education of China (Grant No. 20122304120011), and the Natural Science Foundation of Heilongjiang Province, China (Grant No. QC2014C079), and the Scientific Research Fundation of the Education Department of Heilongjiang Province, China (Grant No. 12541657). The authors would like to thank Professor Sheng-Chun Piao of Harbin Engineering University for his helpful discussion and advice.

Journal of Marine Science and Technology, Vol. 23, No. 2, pp. 151-161 (2015)
DOI: 10.6119/JMST-014-0325-1

ROBUST BEARING ESTIMATION IN SHALLOW WATER USING VECTOR OPTIMIZATION

Hai-Yan Song[1, 2], Jie Shi[3, 4], Chang-Yi Yang[5], Bo-Sheng Liu[4], and Ming Diao[1]

Key words: robust bearing estimation, correlated multi-paths, vector optimization, shallow water.

ABSTRACT

Correlated multi-paths may cause a biased bearing estimation in shallow water, so most existing methods make fully use of the multi-path nature and the underwater channel property to provide an unbiased bearing estimation. However, an imprecise knowledge of the underwater channel parameters or the array model mismatches will cause performance degradation, especially for the high-resolution methods. Therefore development of robust bearing estimation methods in shallow water is critically important. In this paper, a new approach to robust bearing estimation is proposed in the presence of underwater channel parameter uncertainties or array model mismatches. The proposed method is based on the convex optimization theory, exactly to say, the vector optimization theory, and can be derived by imposing a certain constraint on the Euclidean norm of the source vector. It is shown that the proposed method can be reformulated as a convex second-order cone program (SOCP) problem and solved efficiently by the well-established interior point method, such as SEDUMI. Computer simulations and experiment analysis show that the proposed method is highly robust against the underwater channel parameter uncertainties and array model mismatches, moreover, demonstrates its excellent performance as compared with existing methods.

Paper submitted 02/19/13; revised 03/07/14; accepted 03/25/14. Author for correspondence: Jie Shi (e-mail: shijie@hrbeu.edu.cn).
[1] *College of Information And Communication Engineering, Harbin Engineering University, Harbin, China.*
[2] *School of Electrical and Information Engineering, Heilongjiang Institute of Technology, Harbin, China.*
[3] *Acoustic Science and Technology Laboratory, Harbin Engineering University, Harbin, China.*
[4] *College of Underwater Acoustic Engineering, Harbin Engineering University, Harbin, China.*
[5] *Department of Computer Science and Information Engineering, National Penghu University of Science and Technology, Magong, Taiwan, R.O.C.*

I. INTRODUCTION

In the array signal processing domain, the topic of bearing estimation has become an area of active interest with applications in radar, sonar, medical imaging, and other areas (Krim and Viberg, 1996; Li et al., 2007). The conventional time delay methods and a variety of high-resolution methods have been proposed for bearing estimation, such as Multiple Signal Classification (MUSIC) and so on (Xuan et al., 2011). However, due to the multi-path effect in shallow water, the signals from a sound source travel along different paths and tend to be fully or partially correlated, so the above mentioned methods for bearing estimation can no longer perform well (Buckingham, 1984; Karthikeyan, 1986; Carey et al., 2006; Heaney, 2011).

Many approaches have been proposed during the past several decades to tackle the problem of correlated multi-paths in shallow water (Chouhan and Anand, 1993; Krasny and Antonyuk, 1997; Lee et al., 2009; Nagananda and Anand, 2010; Madadi et al., 2011). Among the literature, the concept of Matched Field Processing (MFP) proposed by Bucker is very popular and widely used by many researchers (Baggeroer et al., 1993; Xiao et al., 2009). In MFP, the comparison between the observed signals and the computed acoustic field is based on the classical spatial spectrum estimation algorithms such as Conventional Beamforming (CBF), Standard Capon Beamforming (SCB), and other subspace-based methods (Tolstoy, 1993; Dosso and Wilmut, 2012). However, bearing estimation using MFP requires either a computationally expensive three-dimensional search or a priori knowledge of the source ranges and depths (Naidu and Ganesan, 1995). Several other approaches are known to be able to partly overcome the above problem. Naidu has introduced a new subspace method called Multi-Image Subspace Algorithm (MISA) in which the multi-path correlations are employed for bearing estimation (Naidu, 1991). Lakshmipathi has developed a new high-resolution method called the subspace intersection method to obtain unbiased bearing estimation in shallow water by a one-dimensional search without the prior knowledge of the source ranges and depths (Lakshmipathi and Anand, 2004). Hou et al. (2008) adopted the normal modes sound wave theory and the maxi-

mum likelihood bearing estimation method for target localization in shallow water (Hou et al., 2008).

However, the main shortcoming of the existing approaches is the requirement of a precise knowledge of the underwater channel parameters such as bottom sediment and less robust to the array model mismatches. In such cases, robust approaches to bearing estimation in shallow water are urgently required.

As we all know, Robust Capon Beamforming (RCB) can perform well in the case of the array model mismatches (Vorobyov et al., 2003). The most popular of RCB algorithms include Linearly Constrained Minimum Variance Beamformer (LCMV), Diagonal Loading (DL), Worst-Case Performance Optimization (WCPO), and so on (Yan and Ma, 2005; Zhang et al., 2009). Among them, the LCMV algorithm provides robustness against the signal look direction mismatches (Markovich and Gannot, 2012), and the completion of the DL algorithm depends on the diagonal loading factor (Li et al., 2003), while the WCPO algorithm involves minimization of a quadratic function subject to infinitely many non-convex quadratic constraints (Vorobyov et al., 2003). In an attempt to overcome a substantial degradation of the SCB performance in situations of small training sample size and imprecise knowledge of the Signal Of Interest (SOI) steering vector, a new algorithm called Vector Optimization Robust Beamforming (VORB) is proposed by Song et al. (Song et al., 2012a; Song et al., 2012b), which is simpler and highly robust against the array model mismatches.

In this paper, we demonstrate how VORB can be extended to robust bearing estimation in shallow water in situations of imprecise knowledge of the underwater channel parameters. Briefly, the proposed method in this paper makes explicit use of both the multi-path nature of acoustic propagation in an oceanic waveguide and VORB to provide sufficient robustness improvements for bearing estimation in shallow water. In fact, we prove that the uncertainty set of the array source vector contains not only the array model parameters but also the underwater channel parameters, so the proposed algorithm can be derived by imposing a certain constraint on the Euclidean norm of the source vector. It turns out that our proposed method can be reformulated as a convex second-order cone program (SOCP) and solved efficiently by the well-established interior point method, such as SEDUMI (Sturm, 1999). Moreover, through computer simulations and experiment analysis, we also show a high robustness gain of the proposed method over other traditional techniques.

The content organization is as follows: Section I introduces some background of robust bearing estimation in shallow water. Section II presents the array signal model in shallow water, where the multi-path nature of acoustic propagation in shallow water is considered. In Section III, the multi-path influence to the bearing estimate is analyzed, and the phenomenon for biased bearing estimates is shown. In Section IV, we first describe a new formulation of robust bearing estimation based on VORB in shallow water, and then solve and implement the formulation by SOCP. Section V analyzes the performance of our proposed M-VORB by numerical results in detail. Section VI contains experimental results, where a performance evaluation is presented. The conclusions are summarized in Section VII.

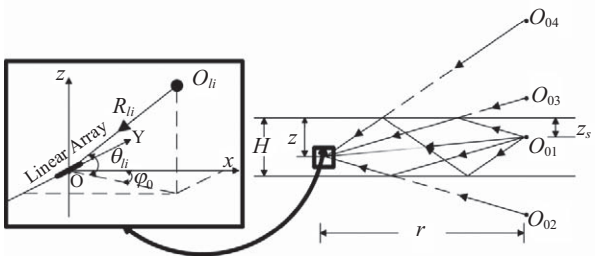

Fig. 1. Array signal model for the signal propagation in a shallow-water channel.

II. ARRAY SIGNAL MODEL IN SHALLOW WATER

As shown in Fig. 1, consider a uniform shallow water channel of depth H meters with a sound source located at z_s meters below the water surface. A linear horizontal array of N equally spaced hydrophones (spacing d) is at a depth of z meters below the surface and r meters horizontally away from the source. Due to the multi-path channel characteristics, there exists a series of significant images whose number tends to infinity.

Suppose the first sensor is the reference element, and its output is given by

$$p(r,z)=\sum_{l=0}^{\infty}\left[(VV_{l1})^l\frac{e^{jkR_{l1}}}{R_{l1}}+(VV_{l2})^lV_{l2}\frac{e^{jkR_{l2}}}{R_{l2}}+(VV_{l3})^lV\frac{e^{jkR_{l3}}}{R_{l3}}+(VV_{l4})^{l+1}\frac{e^{jkR_{l4}}}{R_{l4}}\right] \quad (1)$$

where the notation j represents $\sqrt{-1}$, k is the wave number, R_{li} is the distance from the $l\times i^{\text{th}}$ image to the reference sensor, l represents the order number, i represents the ray number. $V=-1$ is the reflection coefficient for the ray from the sea surface, V_{li} is the reflection coefficient for the $l\times i^{\text{th}}$ ray from the sea bottom. The distance from the $l\times i^{\text{th}}$ image to the n^{th} sensor can be given by

$$R_{li,n}=R_{li}-(n-1)d\sin\varphi_0\cos\theta_{li} \quad (2)$$

where φ_0 is the incident bearing angle, θ_{li} is the elevation angle corresponding to the $l\times i^{\text{th}}$ ray.

The output of the n^{th} sensor can be written as

$$p_n(r,z)=\sum_{l=0}^{\infty}\left[(VV_{l1})^l\frac{e^{jkR_{l1,n}}}{R_{l1,n}}+(VV_{l2})^lV_{l2}\frac{e^{jkR_{l2,n}}}{R_{l2,n}}\right.$$

$$+ (VV_{l3})^l V \frac{\mathrm{e}^{\mathrm{j}kR_{l3,n}}}{R_{l3,n}} + (VV_{l4})^{l+1} \frac{\mathrm{e}^{\mathrm{j}kR_{l4,n}}}{R_{l4,n}} \Bigg] \tag{3}$$

Using Eq. (2), we can convert Eq. (3) into

$$p_n(r,z) =$$

$$\sum_{l=0}^{\infty} \Bigg[(VV_{l1})^l \frac{\mathrm{e}^{\mathrm{j}kR_{l1}} e^{-jk(n-1)d\sin\varphi_0\cos\theta_{l1}}}{R_{l1,n}} + (VV_{l2})^l V_{l2} \frac{\mathrm{e}^{\mathrm{j}kR_{l2}} e^{-jk(n-1)d\sin\varphi_0\cos\theta_{l2}}}{R_{l2,n}}$$

$$+ (VV_{l3})^l V \frac{\mathrm{e}^{\mathrm{j}kR_{l3}} e^{-jk(n-1)d\sin\varphi_0\cos\theta_{l3}}}{R_{l3,n}} + (VV_{l4})^{l+1} \frac{\mathrm{e}^{\mathrm{j}kR_{l4}} e^{-jk(n-1)d\sin\varphi_0\cos\theta_{l4}}}{R_{l4,n}} \Bigg] \tag{4}$$

when $d \ll r$, Eq. (4) can be approximated as

$$p_n(r,z) \approx$$

$$\sum_{l=0}^{\infty} \Bigg[(VV_{l1})^l \frac{\mathrm{e}^{\mathrm{j}kR_{l1}} e^{-jk(n-1)d\sin\varphi_0\cos\theta_{l1}}}{R_{l1}} + (VV_{l2})^l V_{l2} \frac{\mathrm{e}^{\mathrm{j}kR_{l2}} e^{-jk(n-1)d\sin\varphi_0\cos\theta_{l2}}}{R_{l2}}$$

$$+ (VV_{l3})^l V \frac{\mathrm{e}^{\mathrm{j}kR_{l3}} e^{-jk(n-1)d\sin\varphi_0\cos\theta_{l3}}}{R_{l3}} + (VV_{l4})^{l+1} \frac{\mathrm{e}^{\mathrm{j}kR_{l4}} e^{-jk(n-1)d\sin\varphi_0\cos\theta_{l4}}}{R_{l4}} \Bigg] \tag{5}$$

Let us express Eq. (5) in a matrix notation

$$p_n(r,z) = \sum_{l=0}^{\infty} \boldsymbol{A}_{nl} \boldsymbol{W}_l \tag{6}$$

$$\boldsymbol{W}_l = \begin{bmatrix} (VV_{l1})^l \dfrac{\mathrm{e}^{\mathrm{j}kR_{l1}}}{R_{l1}} \\ (VV_{l2})^l V_{l2} \dfrac{\mathrm{e}^{\mathrm{j}kR_{l2}}}{R_{l2}} \\ (VV_{l3})^l V \dfrac{\mathrm{e}^{\mathrm{j}kR_{l3}}}{R_{l3}} \\ (VV_{l4})^{l+1} \dfrac{\mathrm{e}^{\mathrm{j}kR_{l4}}}{R_{l4}} \end{bmatrix} \tag{7}$$

$$\boldsymbol{A}_{nl} = \begin{bmatrix} e^{-jk(n-1)d\sin\varphi_0\cos\theta_{l1}} \\ e^{-jk(n-1)d\sin\varphi_0\cos\theta_{l2}} \\ e^{-jk(n-1)d\sin\varphi_0\cos\theta_{l3}} \\ e^{-jk(n-1)d\sin\varphi_0\cos\theta_{l4}} \end{bmatrix} \tag{8}$$

where $\boldsymbol{W}_l$ is the weight vector corresponding to the l^{th} image, $\boldsymbol{A}_{nl}$ is the image space spanned by the l^{th} image on the n^{th} sensor.

So the output of the horizontal linear array in shallow water can be represented as

$$\boldsymbol{X}(t) = \begin{bmatrix} \boldsymbol{x}_1(t) \\ \boldsymbol{x}_2(t) \\ \vdots \\ \boldsymbol{x}_N(t) \end{bmatrix} = \begin{bmatrix} P_1(r,z) \\ P_2(r,z) \\ \vdots \\ P_N(r,z) \end{bmatrix} \boldsymbol{s}(t) = \begin{bmatrix} \sum_{l=1}^{\infty} \boldsymbol{A}_{1l} \boldsymbol{W}_l \\ \sum_{l=1}^{\infty} \boldsymbol{A}_{2l} \boldsymbol{W}_l \\ \vdots \\ \sum_{l=1}^{\infty} \boldsymbol{A}_{Nl} \boldsymbol{W}_l \end{bmatrix} \boldsymbol{s}(t) \tag{9}$$

where $\boldsymbol{s}(t)$ represents the original transmitting signal. Eq. (9) can be further written in a compact form

$$\boldsymbol{X}(t) = \boldsymbol{B}\boldsymbol{s}(t) = \sum_{l=0}^{\infty} \left[\boldsymbol{B}_l \right] \boldsymbol{s}(t) = \sum_{l=0}^{\infty} \left[\boldsymbol{A}_l \boldsymbol{W}_l \right] \boldsymbol{s}(t) \tag{10}$$

$$\boldsymbol{A}_l = \left[\boldsymbol{a}_{l1}, \boldsymbol{a}_{l2}, \boldsymbol{a}_{l3}, \boldsymbol{a}_{l4} \right] \tag{11}$$

where $\boldsymbol{a}_{li} = \left[1, e^{-jkd\sin\varphi_0\cos\theta_{li}}, \cdots, e^{-jk(N-1)d\sin\varphi_0\cos\theta_{li}} \right]^{\mathrm{T}}$, $\boldsymbol{A}_l$ is the image space spanned by the l^{th} image, $\boldsymbol{B}_l$ is the source vector corresponding to the l^{th} image, $\boldsymbol{B}$ is the source vector.

When $l = 0$, only consider the four rays from the 0^{th} image, and the array signal model can be simplified as

$$\boldsymbol{X}(t) = \boldsymbol{B}_0 \boldsymbol{s}(t) = \boldsymbol{A}_0 \boldsymbol{W}_0 \boldsymbol{s}(t) \tag{12}$$

$$\boldsymbol{A}_0 = \left[\boldsymbol{a}_{01}, \boldsymbol{a}_{02}, \boldsymbol{a}_{03}, \boldsymbol{a}_{04} \right] \tag{13}$$

$$\boldsymbol{W}_0 = \left[\frac{\mathrm{e}^{\mathrm{j}kR_{01}}}{R_{01}}, V_{02} \frac{\mathrm{e}^{\mathrm{j}kR_{02}}}{R_{02}}, V \frac{\mathrm{e}^{\mathrm{j}kR_{03}}}{R_{03}}, VV_{04} \frac{\mathrm{e}^{\mathrm{j}kR_{04}}}{R_{04}} \right]^{\mathrm{T}} \tag{14}$$

From the above mentioned equations, we can see that due to the multi-path nature of acoustic propagation in the ocean, the structure of the source vector is obviously different from that of the steering vector in conventional array signal model. It is just the reason why the plane-wave DOA estimation techniques, such as CBF, SCB and so on, yield biased bearing estimation in shallow water.

III. MULTI-PATH INFLUENCE TO THE BEARING ESTIMATE

1. Theoretical Analysis

As we all know, conventional bearing estimation methods are based on the plane-wave assumption, and the output of the array of narrowband sensors can be expressed as the vector

$$\boldsymbol{X}'(t) = \left[x_1'(t), x_2'(t), \cdots, x_N'(t) \right]^{\mathrm{T}} = \boldsymbol{A}'(\varphi_0)\boldsymbol{s}(t) \tag{15}$$

where $\boldsymbol{A}'(\varphi_0) = \left[1, e^{-jkd\sin\varphi_0}, \cdots, e^{-jk(N-1)d\sin\varphi_0} \right]^{\mathrm{T}}$ is the array

steeing vector, and $k = \omega/c$ is the wave number.

For the conventional beamformer, the weight vector $\boldsymbol{w}(\varphi) = \left[1, e^{-jkd\sin\varphi}, \cdots, e^{-jk(N-1)d\sin\varphi}\right]^{\mathrm{T}}$ is chosen, and the average output power of the array in the direction of bearing angle φ can be expressed as

$$P(\varphi) = E\left\{\left[\boldsymbol{w}^{\mathrm{H}}(\varphi)\boldsymbol{A}'(\varphi_0)\boldsymbol{s}(t)\right]\left[\boldsymbol{w}^{\mathrm{H}}(\varphi)\boldsymbol{A}'(\varphi_0)\boldsymbol{s}(t)\right]^{\mathrm{H}}\right\}$$
$$= \left[\boldsymbol{w}^{\mathrm{H}}(\varphi)\boldsymbol{A}'(\varphi_0)\right]E\left\{\boldsymbol{s}(t)\boldsymbol{s}^{\mathrm{H}}(t)\right\}\left[\boldsymbol{w}^{\mathrm{H}}(\varphi)\boldsymbol{A}'(\varphi_0)\right]^{\mathrm{H}} \quad (16)$$

Eq. (16) shows that when φ equals to φ_0 ($\varphi = \varphi_0$), the average output power $P(\varphi)$ reaches the maximum, and then the bearing estimate φ_0 is provided by the position of the maximum peak in the spatial spectrum map.

However, when the incident signal comes from the multi-path propagation as shown in Eq. (12), the average output power of the array in the direction of bearing angle φ will alternately be expressed as

$$P(\varphi) = E\left\{\left[\boldsymbol{w}^{\mathrm{H}}(\varphi)\boldsymbol{X}(t)\right]\left[\boldsymbol{w}^{\mathrm{H}}(\varphi)\boldsymbol{X}(t)\right]^{\mathrm{H}}\right\}$$
$$= E\left\{\left[\boldsymbol{w}^{\mathrm{H}}(\varphi)\boldsymbol{B}_0\boldsymbol{s}(t)\right]\left[\boldsymbol{w}^{\mathrm{H}}(\varphi)\boldsymbol{B}_0\boldsymbol{s}(t)\right]^{\mathrm{H}}\right\}$$
$$= E\left\{\left[\boldsymbol{w}^{\mathrm{H}}(\varphi)\boldsymbol{A}_0\boldsymbol{W}_0\boldsymbol{s}(t)\right]\left[\boldsymbol{w}^{\mathrm{H}}(\varphi)\boldsymbol{A}_0\boldsymbol{W}_0\boldsymbol{s}(t)\right]^{\mathrm{H}}\right\}$$
$$= \left[\boldsymbol{w}^{\mathrm{H}}(\varphi)\boldsymbol{A}_0\right]E\left\{\left[\boldsymbol{W}_0\boldsymbol{s}(t)\right]\left[\boldsymbol{W}_0\boldsymbol{s}(t)\right]^{\mathrm{H}}\right\}\left[\boldsymbol{w}^{\mathrm{H}}(\varphi)\boldsymbol{A}_0\right]^{\mathrm{H}} \quad (17)$$

where

$$\boldsymbol{A}_0 = \left[\boldsymbol{A}_{01}, \boldsymbol{A}_{02}, \boldsymbol{A}_{03}, \boldsymbol{A}_{04}\right] \quad (18)$$

$$\boldsymbol{A}_{0m} = \left[1, e^{-jkd\sin\varphi_0\cos\theta_{0m}}, \cdots, e^{-jk(N-1)d\sin\varphi_0\cos\theta_{0m}}\right]^{\mathrm{T}} \quad (19)$$

where $m = 1, 2, 3, 4$. Take Eq. (18) and Eq. (19) into account, and we can rewrite Eq. (17) as

$$P(\varphi) = \sum_{m=1}^{4}\left[\boldsymbol{w}^{\mathrm{H}}(\varphi)\boldsymbol{A}_{0m}\right]E\left\{\left[\boldsymbol{W}_0\boldsymbol{s}(t)\right]\left[\boldsymbol{W}_0\boldsymbol{s}(t)\right]^{\mathrm{H}}\right\}\left[\boldsymbol{w}^{\mathrm{H}}(\varphi)\boldsymbol{A}_{0m}\right]^{\mathrm{H}} \quad (20)$$

Then Eq. (20) can be expressed as a contracted form

$$P(\varphi) = \sum_{m=1}^{4} P_m(\varphi) \quad (21)$$

where $P_m(\varphi)$ denotes the average output power of the array due to the m^{th} eigenray

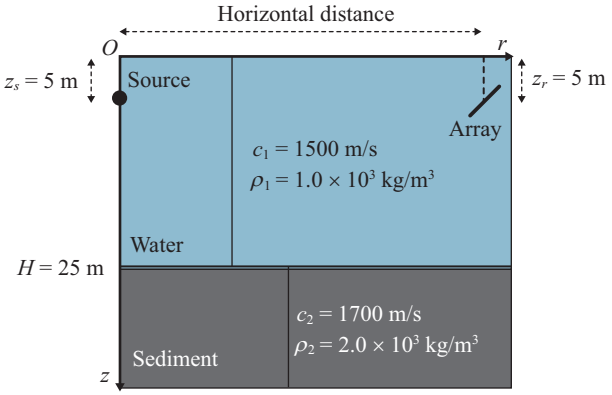

Fig. 2. A Pekeris channel in shallow water.

$$P_m(\varphi) = \left[\boldsymbol{w}^{\mathrm{H}}(\varphi)\boldsymbol{A}_{0m}\right]E\left\{\left[\boldsymbol{W}_0\boldsymbol{s}(t)\right]\left[\boldsymbol{W}_0\boldsymbol{s}(t)\right]^{\mathrm{H}}\right\}\left[\boldsymbol{w}^{\mathrm{H}}(\varphi)\boldsymbol{A}_{0m}\right]^{\mathrm{H}} \quad (22)$$

Eq. (22) can be further transformed to the following form

$$P_m(\varphi) = \left[1 + \cdots + e^{jk(N-1)d(\sin\varphi - \sin\varphi_0\cos\theta_{0m})}\right]$$
$$E\left\{\left[\boldsymbol{W}_0\boldsymbol{s}(t)\right]\left[\boldsymbol{W}_0\boldsymbol{s}(t)\right]^{\mathrm{H}}\right\}\left[1 + \cdots + e^{jk(N-1)d(\sin\varphi - \sin\varphi_0\cos\theta_{0m})}\right]^{\mathrm{H}} \quad (23)$$

From above equations, it can easily be seen that under the conditions of multi-paths, each eigenray makes a contribution to the average output power of the array. If the elevation angle $\theta_{0m} = 0°$ ($m = 1, 2, 3, 4$) and $\cos\theta_{0m} = 1$, $\boldsymbol{A}_{0m}$ will be equivalent to $\boldsymbol{A}'(\varphi_0)$. Then the same bearing estimate φ_0 will be provided by the position of the maximum peak of each $P_m(\varphi)$, and the superposition of $P_m(\varphi)$ will, of course, indicate the correct bearing estimate φ_0. Consequently, there exists no biased bearing estimate.

However, due to the practical multi-path propagation in underwater acoustic channel in shallow water, the elevation angle θ_{0m} ($m = 1, 2, 3, 4$) no longer equals to zero (which means $\theta_{0m} \neq 0°$ and $\cos\theta_{0m} \neq 1$). So each $P_m(\varphi)$ is different and the superposition of $P_m(\varphi)$ will no longer indicate the correct bearing estimate φ_0. Consequently, there appears biased bearing estimate.

2. Numerical Analysis

As shown in Fig. 2, the ocean model is an ideal Pekeris channel, where water depth is 25 m, sound speed in water is 1500 m/s, density of the water is 1.0×10^3 kg/m^3, sound speed in sediment is 1700 m/s, density of the sediment is 2.0×10^3 kg/m^3. The sound source is at a depth of 5 m below the water surface. The horizontal uniform linear array with 24 sensors and half-wavelength sensor spacing is also located at 5 m below the surface. Assume signal frequency is 100 kHz, the incident bearing is $\varphi = 25°$ or $\varphi = 35°$, the horizontal distance

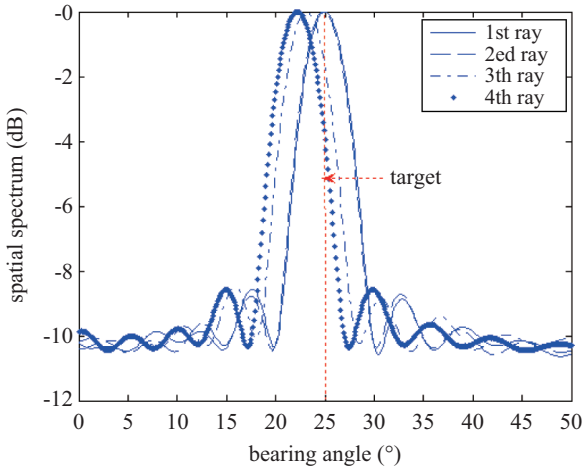

(a) R = 100 m φ = 25°

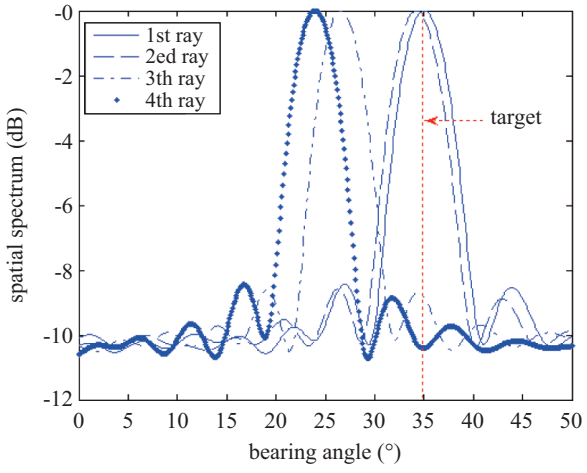

(b) R = 50 m φ = 35°

Fig. 3. The bearing estimation results for different eigenrays.

between the source and the array is R = 100 m or R = 50 m, the snapshots number is 1024, Signal to Noise Ratio (SNR) is 10 dB.

Fig. 3 shows the spatial spectrums by CBF respectively for the first four eigenrays. Note that the incident bearing is denoted by a vertical red dotted line, and each eigenray has a different spatial spectrum whose peak indicates a mismatch bearing angle against the actual incident angle. As discussed above, the spectrum superposition must indicate a biased bearing estimate, which will be depicted in Section V.

Extensive simulation has been carried out to compute the bearing estimate biases by CBF as a function of different incidence angles in Fig. 4. The biases are computed by averaging over 100 Monte Carlo simulations, and the corresponding results respectively for R = 50 m, 100 m, 150 m, 200 m are given in this figure for comparison. We can see that the estimate bias increases as the incidence bearing angle increases under the conditions of the same horizontal distance, while the estimate bias increases as the horizontal distance decreases under the conditions of the same incidence bearing angle.

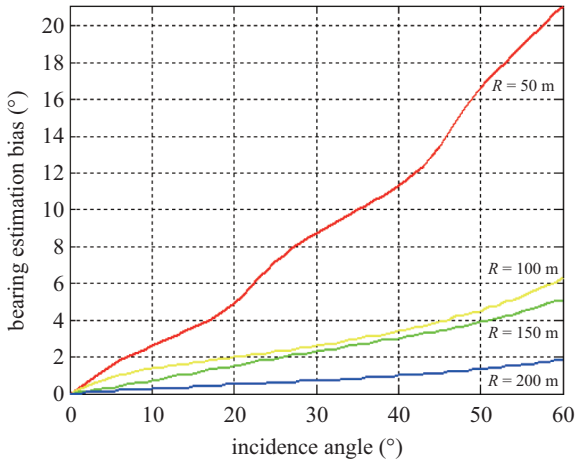

Fig. 4. The bearing estimate biases as a function of different incidence angles.

IV. ROBUST BEARING ESTIMATION ALGORITHM IN SHALLOW WATER

1. Formulation

Below, we provide a robust bearing estimation algorithm using VORB following exactly the same procedure in Song et al. (2012a; 2012b), Vorobyov et al. (2003). In practical applications, there must exist a distortion of source vector due to the underwater channel parameters and array model mismatches. So we assume the source vector distortion to be $\boldsymbol{\Delta}_{\mathrm{M}}$ (the subscript M represents Multi-path for convenience, the following is the same) whose norm can be bounded by a certain constant $\varepsilon > 0$, that is

$$\left\|\boldsymbol{\Delta}_{\mathrm{M}}\right\| \le \varepsilon \tag{24}$$

Then the actual source vector $\boldsymbol{B}_0(\varphi)$ belongs to the following set

$$\boldsymbol{C}_{\mathrm{M}}(\varepsilon \mid \varphi) = \left\{ \boldsymbol{B}_0(\varphi) \mid \boldsymbol{B}_0(\varphi) = \boldsymbol{B}_0^{'}(\varphi) + \boldsymbol{\Delta}_{\mathrm{M}}, \left\|\boldsymbol{\Delta}_{\mathrm{M}}\right\| \le \varepsilon \right\} \tag{25}$$

where $\|\bullet\|$ denotes the norm, $\boldsymbol{B}_0^{'}(\varphi)$ is the theoretic source vector, $\boldsymbol{C}_{\mathrm{M}}(\varepsilon \mid \varphi)$ indicates the uncertainty set whose elements represent possible mismatches.

Let's impose a constraint on the absolute value of the array response, that is, the value should be larger than or equal to one for all vectors that belong to $\boldsymbol{C}_{\mathrm{M}}(\varepsilon \mid \varphi)$

$$\left|\boldsymbol{w}_{\mathrm{M}}^{\mathrm{H}}(\varphi)\boldsymbol{B}_0(\varphi)\right| \ge 1, \text{ for all } \boldsymbol{B}_0(\varphi) \in \boldsymbol{C}_{\mathrm{M}}(\varepsilon \mid \varphi) \tag{26}$$

where $\boldsymbol{w}_{\mathrm{M}}(\varphi)$ is the weight vector.

So the formulation of robust bearing estimation algorithm can be written as the following constrained optimization problem

$$\begin{cases} \min\limits_{\boldsymbol{w}_{\mathrm{M}}(\varphi)} \quad \boldsymbol{w}_{\mathrm{M}}^{\mathrm{H}}(\varphi)\boldsymbol{R}\boldsymbol{w}_{\mathrm{M}}(\varphi) \\ \text{s.t.} \quad \left|\boldsymbol{w}_{\mathrm{M}}^{\mathrm{H}}(\varphi)\boldsymbol{B}_0(\varphi)\right| \geq 1 \quad for \quad all \quad \boldsymbol{B}_0(\varphi) \in \boldsymbol{C}_{\mathrm{M}}(\varepsilon \mid \varphi) \end{cases} \tag{27}$$

We can rewrite the problem (27) as

$$\begin{cases} \min\limits_{\boldsymbol{w}_{\mathrm{M}}(\varphi)} \quad \boldsymbol{w}_{\mathrm{M}}^{\mathrm{H}}(\varphi)\boldsymbol{R}\boldsymbol{w}_{\mathrm{M}}(\varphi) \\ \text{s.t.} \quad \boldsymbol{w}_{\mathrm{M}}^{\mathrm{H}}(\varphi)\boldsymbol{B}_0^{'}(\varphi) \geq \varepsilon \left\|\boldsymbol{w}_{\mathrm{M}}(\varphi)\right\| + 1, \quad \mathrm{Im}\left\{\boldsymbol{w}_{\mathrm{M}}^{\mathrm{H}}(\varphi)\boldsymbol{B}_0^{'}(\varphi)\right\} = 0 \end{cases} \tag{28}$$

where $\boldsymbol{R}$ is the covariance matrix. Make explicit use of the idea of VORB and the nature of multi-path channel, then we can reformulate the optimization problem as

$$\begin{cases} \min\limits_{\boldsymbol{w}_{\mathrm{M}}(\varphi)} \quad (w.r.t.\boldsymbol{R}_{+}^{2}) \quad (\left\|\boldsymbol{U}\boldsymbol{w}_{\mathrm{M}}(\varphi)\right\|_2, \left\|\boldsymbol{w}_{\mathrm{M}}(\varphi)\right\|_2) \\ \text{s.t.} \quad \boldsymbol{w}_{\mathrm{M}}^{\mathrm{H}}(\varphi)\boldsymbol{B}_0^{'}(\varphi) \geq \varepsilon \left\|\boldsymbol{w}_{\mathrm{M}}(\varphi)\right\| + 1, \quad \mathrm{Im}\left\{\boldsymbol{w}_{\mathrm{M}}^{\mathrm{H}}(\varphi)\boldsymbol{B}_0^{'}(\varphi)\right\} = 0 \end{cases} \tag{29}$$

where *w.r.t.* is the abbreviation for "with respect to", $\boldsymbol{R}_{+}^{2}$ means that the values of the objective functions $\left\|\boldsymbol{U}\boldsymbol{w}_{\mathrm{M}}(\varphi)\right\|_2$ and $\left\|\boldsymbol{w}_{\mathrm{M}}(\varphi)\right\|_2$ should be discussed in the set of positive numbers, $\boldsymbol{U}$ is the Cholesky factorization factor which can be represented as

$$\boldsymbol{R} = \boldsymbol{U}^{\mathrm{H}}\boldsymbol{U} \tag{30}$$

Eq. (29) is just our proposed algorithm called Multi-path based Vector Optimization Robust Beamforming (for abbreviation: M-VORB) in this paper, which is a vector optimization problem who belongs to a bi-criterion problem. $\left\|\boldsymbol{w}_{\mathrm{M}}(\varphi)\right\|_2$ is the penalty function, which can help us to obtain the robust weight vector $\boldsymbol{w}_{\mathrm{M}}(\varphi)$ under the conditions that there exists some disturbs in $\boldsymbol{U}$.

2. Solution and Implementation by SOCP

According to the regularized approximation (Boyd and Vandenberghe, 2006), (29) can be reformulated as

$$\begin{cases} \min\limits_{\boldsymbol{w}_{\mathrm{M}}(\varphi)} \quad (\left\|\boldsymbol{U}\boldsymbol{w}_{\mathrm{M}}(\varphi)\right\|_2 + \gamma \left\|\boldsymbol{w}_{\mathrm{M}}(\varphi)\right\|_2) \\ \text{s.t.} \quad \boldsymbol{w}_{\mathrm{M}}^{\mathrm{H}}(\varphi)\boldsymbol{B}_0^{'}(\varphi) \geq \varepsilon \left\|\boldsymbol{w}_{\mathrm{M}}(\varphi)\right\| + 1, \quad \mathrm{Im}\left\{\boldsymbol{w}_{\mathrm{M}}^{\mathrm{H}}(\varphi)\boldsymbol{B}_0^{'}(\varphi)\right\} = 0 \end{cases} \tag{31}$$

where $\gamma > 0$ is the constraint parameter. Introduce two non-negative scalars t_1, t_2 and two new constraints $\left\|\boldsymbol{U}\boldsymbol{w}_{\mathrm{M}}(\varphi)\right\|_2 \leq t_1$, $\left\|\boldsymbol{w}_{\mathrm{M}}(\varphi)\right\|_2 \leq t_2$, then we can convert Eq. (31) into the following problem

$$\begin{cases} \min\limits_{\boldsymbol{w}_{\mathrm{M}}(\varphi)} \quad (t_1 + \gamma t_2) \\ \text{s.t.} \quad \left\|\boldsymbol{U}\boldsymbol{w}_{\mathrm{M}}(\varphi)\right\|_2 \leq t_1, \quad \left\|\boldsymbol{w}_{\mathrm{M}}(\varphi)\right\|_2 \leq t_2, \\ \qquad \varepsilon \left\|\boldsymbol{w}_{\mathrm{M}}(\varphi)\right\|_2 \leq \boldsymbol{w}_{\mathrm{M}}^{\mathrm{H}}(\varphi)\boldsymbol{B}_0^{'}(\varphi) - 1, \ \mathrm{Im}(\boldsymbol{w}_{\mathrm{M}}^{\mathrm{H}}(\varphi)\boldsymbol{B}_0^{'}(\varphi)) = 0 \end{cases} \tag{32}$$

Let

$$\boldsymbol{y}_{\mathrm{M}} = [t_1, t_2, \boldsymbol{w}_{\mathrm{M}}^{\mathrm{T}}(\varphi)]^{\mathrm{T}} \tag{33}$$

$$\boldsymbol{b}_{\mathrm{M}} = [1, \gamma, \boldsymbol{0}_{N\times 1}{}^{\mathrm{T}}]^{\mathrm{T}} \tag{34}$$

$$\boldsymbol{f}_{\mathrm{M}} \triangleq [\boldsymbol{0}_{(2N+2)\times 1}{}^{\mathrm{T}}, -1, \boldsymbol{0}_{N\times 1}{}^{\mathrm{T}}]^{\mathrm{T}} \in \boldsymbol{R}^{(3\times N+3)\times 1} \tag{35}$$

$$\boldsymbol{F}_{\mathrm{M}}^{\mathrm{T}} \triangleq \begin{bmatrix} 1 & 0 & \boldsymbol{I}_{1\times N} \\ \boldsymbol{0}_{N\times 1} & \boldsymbol{0}_{N\times 1} & \boldsymbol{U}_{N\times N} \\ 0 & 1 & \boldsymbol{0}_{1\times N} \\ \boldsymbol{0}_{N\times 1} & \boldsymbol{0}_{N\times 1} & \boldsymbol{I}_{N\times N} \\ 0 & 0 & \boldsymbol{B}_0^{'\mathrm{H}}(\varphi) \\ \boldsymbol{0}_{N\times 1} & \boldsymbol{0}_{N\times 1} & \varepsilon \boldsymbol{I}_{N\times N} \end{bmatrix} \tag{36}$$

Eq. (29) can be further transformed into the SOCP form

$$\begin{cases} \min\limits_{\boldsymbol{y}} \quad \boldsymbol{b}_{\mathrm{M}}^{\mathrm{T}}\boldsymbol{y}_{\mathrm{M}} \\ \text{s.t.} \quad \boldsymbol{f}_{\mathrm{M}} + \boldsymbol{F}_{\mathrm{M}}^{\mathrm{T}}\boldsymbol{y}_{\mathrm{M}} \in SOC_1^{N+1} \times SOC_2^{N+1} \times SOC_3^{N+1} \end{cases} \tag{37}$$

So we can easily solve Eq. (37) by the mathematical software tool SEDUMI (Sturm, 1999), and obtain the optimization weight vector $\boldsymbol{w}_{\text{M-opt}}(\varphi)$.

3. The Proposed Algorithm Flow

The M-VORB algorithm for bearing estimation may be described as follows:

(1) Estimate the sample covariance matrix $\hat{\boldsymbol{R}}$ from the array data vector $\boldsymbol{X}(t)$ by $\hat{\boldsymbol{R}} = \boldsymbol{X}(t)\boldsymbol{X}^{\mathrm{H}}(t)/L$.
(2) Do the Cholesky factorization of $\hat{\boldsymbol{R}}$ as Eq. (30), and obtain the Cholesky factorization factor $\boldsymbol{U}$.
(3) According to Eq. (12)-(14), construct the theoretic source vector $\boldsymbol{B}_0^{'}(\varphi)$.
(4) Set the constant ε (which is used to bound the norm of the source vector distortion) and the constraint parameter γ (which is used for the regularized approximation).
(5) Form the matrices $\boldsymbol{b}_{\mathrm{M}}$, $\boldsymbol{f}_{\mathrm{M}}$ and $\boldsymbol{F}_{\mathrm{M}}^{\mathrm{T}}$ by Eqs. (34)-(36).
(6) Compute Eq. (37) by the mathematical software tool SEDUMI and obtain the optimization weight vector $\boldsymbol{w}_{\text{M-opt}}(\varphi)$.
(7) Substitute $\boldsymbol{w}_{\text{M-opt}}(\varphi)$ for $\boldsymbol{w}$ in $\boldsymbol{w}^{\mathrm{H}}\boldsymbol{R}\boldsymbol{w}$, and compute the

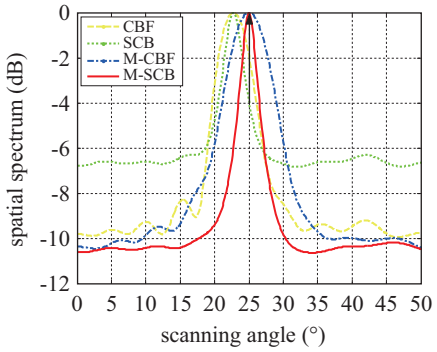

(a) R = 100 m φ = 25°

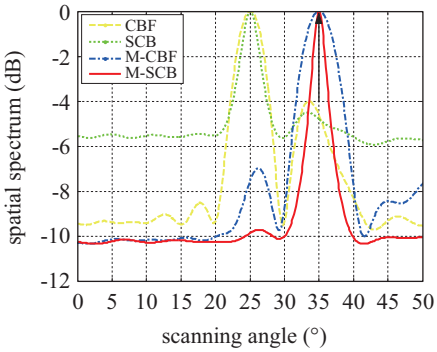

(b) R = 50 m φ = 35°

Fig. 5. The spatial spectrums of CBF, SCB, M-CBF and M-SCB.

function $P_{\text{M-VORB}}(\varphi) = \boldsymbol{w}_{\text{M-opt}}^{\text{H}}(\varphi)\boldsymbol{R}\boldsymbol{w}_{\text{M-opt}}(\varphi)$.

(8) Scan the spectrum peaks in our interested angular scope, the location of the peaks of $P_{\text{M-VORB}}(\varphi)$ provides estimates of the source bearing angles.

V. NUMERICAL AND EXPERIMENTAL RESULTS

In Section V, we firstly show that a plane-wave assumption leads to biased bearing estimates, and then discuss and analyze the performance of M-VORB under the conditions of the water depth uncertainty and the sediment parameter uncertainty respectively. For convenience, M-CBF is the abbreviation for "Multi-path based Conventional Beamforming", and M-SCB stands for "Multi-path based Standard Capon Beamforming".

1. Spatial Spectrums Analysis for M-CBF and M-SCB

Simulation conditions are similar to Section III. Fig. 5 depicts the spatial spectrums of CBF, SCB, M-CBF and M-SCB, which are respectively denoted by different color lines. Note that the black single-headed arrow indicates the actual bearing angle. We can see that under the multi-paths, the bearing estimate algorithms based on a plane-wave assumption, such as CBF and SCB, can no longer obtain an unbiased bearing estimation. While the multi-path based algorithms such as M-CBF and M-SCB, which make explicit use of the multi-path nature for bearing estimate, can obtain an unbiased bearing estimate.

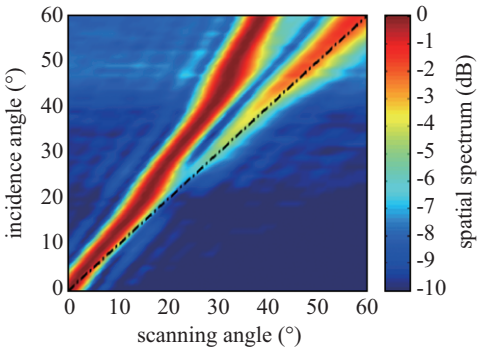

(a) CBF

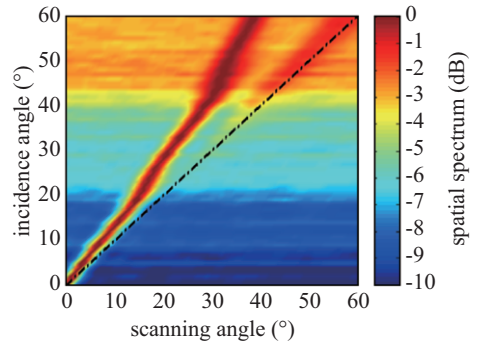

(b) SCB

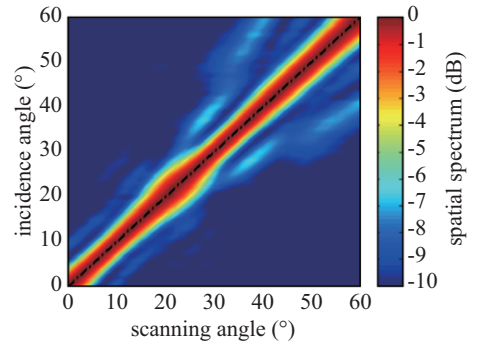

(c) M-CBF

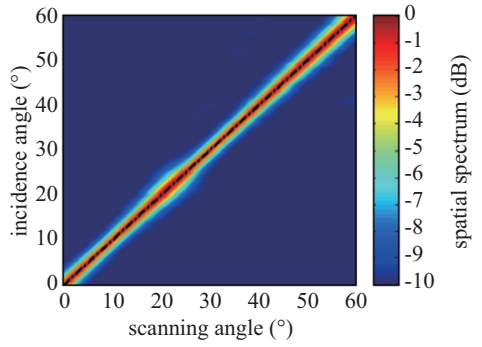

(d) M-SCB

Fig. 6. The 2-Dimension spatial spectrums (R = 50 m).

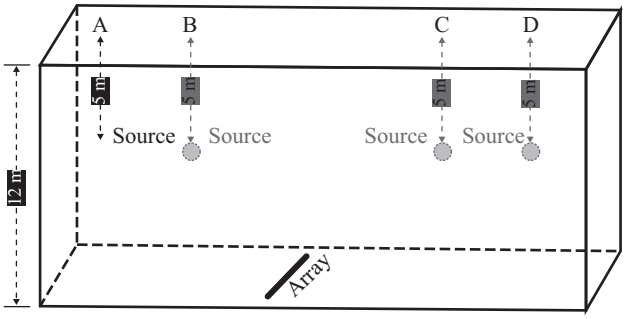

Fig. 7. A source and a array in Pekris channel.

2. Spatial Spectrums Variations versus Incidence Bearing Angle

In this simulation, we will show the spatial spectrums variations versus incidence bearing angle in detail. Simulation conditions are the same, except the incident bearing angle changes from 0° to 60° and $R = 50$ m.

Fig. 6(a) and (b) show the 2-Dimention spatial spectrums versus incidence bearing angles respectively for CBF and SCB, and the actual angle is denoted by the dashed black line. Note that there exist obvious bearing biases when the signal impinges on the array in large incidence angles. This phenomenon indicates that the conventional plane-wave based methods can no longer be suitable to bearing estimation under the multi-paths conditions.

On the other hand, Fig. 6(c) and (d) show the 2-Dimention spatial spectrums respectively for M-CBF and M-SCB. By comparison, we can see that due to the utilization of the multi-path nature, multi-path based methods can accurately estimate the bearing angle even when the incidence signal is closer to the endfire direction.

Simulation results show the multi-path based methods outperform the plane-wave based methods under the condition of multi-paths.

3. Experimental Results

In this section, the multi-path influence to the bearing estimate in shallow water is validated by experimental analysis. For convenience, C-based is the abbreviation for "Conventional plane-wave based methods", and M-based is the abbreviation for "Multi-path based methods".

The experimental data discussed in this paper were collected in a shallow ocean which can be considered as a Pekris channel. The water depth was 12 m, and the wideband sound source was located at 5 m below the sea surface. The horizontal uniform array with fifteen sensors was deployed at a depth of 10 m, and was moored for stable operation. Several elements did not work properly and will be excluded from data analysis. The sound source was respectively located at Point A, B, C, and D as shown in Fig. 7, and the horizontal distances between the location points and the array were respectively 18.7 m, 7.8 m, 7.8 m, and 18.7 m. By the calculation of the formula d^2/λ, the source was considered in the far field of the array. The signal waveform of the reference element is shown in Fig. 8.

Table 1. Numerical results for the bearing estimate (unit: degree).

Localization / Frequency	A		B	
	C-based	M-based	C-based	M-based
80 Hz	-9.00	-9.79	-6.44	-10.29
100 Hz	-5.73	-6.34	-4.41	-7.24
125 Hz	-3.48	-3.94	-0.63	-1.08
160 Hz	***-3.11***	***-3.56***	-1.87	-1.12
200 Hz	-0.64	-0.74	-0.14	-0.20
250 Hz	-0.86	-0.98	-1.44	-1.78
315 Hz	-0.21	-0.75	-0.19	-0.21
400 Hz	-6.80	-7.01	-1.81	-2.95
Localization / Frequency	C		D	
	C-based	M-based	C-based	M-based
80 Hz	-3.76	-6.01	-3.75	-4.08
100 Hz	-3.05	-5.00	-1.63	-1.80
125 Hz	-2.36	-4.00	-2.67	-3.02
160 Hz	0.88	0.41	1.64	1.88
200 Hz	1.60	2.28	1.91	2.19
250 Hz	0.74	0.90	2.79	3.22
315 Hz	1.06	1.29	1.05	1.12
400 Hz	2.39	3.90	1.64	1.79

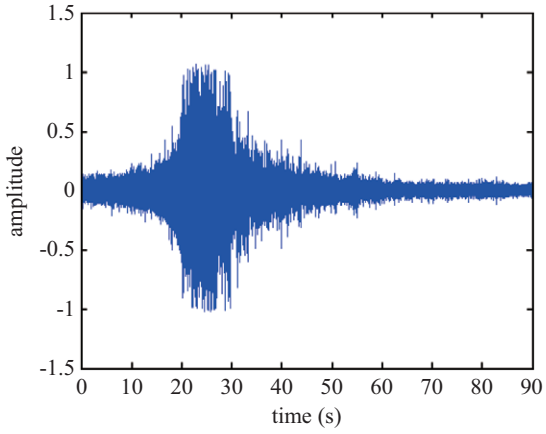

Fig. 8. The signal waveform from the reference element.

For the sake of computational simplicity, we shall henceforth confine our attentions to different 1/3 oct signals. Firstly, according to the above mentioned experimental conditions, the 100 Monte Carlo simulations are done, and the numerical results of C-based and M-based processors are compared in Table 1.

It is noted from Table 1 that, due to the multi-paths, there exist obvious bearing estimate biases. For example, with respect to 160 Hz at location A, the C-based estimate is –3.11°, while the M-based estimate is –3.56° as shown in bolds and italics.

Table 2. The bearing estimation results for experiment (unit: degree).

Localization / Frequency	A		B	
	C-based	M-based	C-based	M-based
80 Hz	-8.81	-9.76	-6.44	-10.32
100 Hz	-5.62	-6.34	-4.51	-7.25
125 Hz	-3.49	-3.96	-1.20	-1.12
160 Hz	***-3.24***	***-3.57***	-4.24	-1.12
200 Hz	-0.62	-0.73	-0.05	-0.20
250 Hz	-0.95	-0.97	-1.81	-1.76
315 Hz	-0.15	-0.78	0.39	-0.22
400 Hz	-5.19	-7.05	-2.12	-2.98
Localization / Frequency	C		D	
	C-based	M-based	C-based	M-based
80 Hz	-3.74	-6.02	-3.82	-4.08
100 Hz	-2.98	-4.99	-1.67	-1.82
125 Hz	-3.13	-4.05	-2.66	-3.00
160 Hz	0.94	0.40	1.50	1.87
200 Hz	1.89	2.27	1.91	2.22
250 Hz	0.71	0.94	2.75	3.22
315 Hz	0.72	1.29	2.09	1.13
400 Hz	2.67	3.98	1.91	1.80

Experimental results are shown in Table 2. It is noteworthy that there are almost no difference as compared with Table 1. Experimental results as well as many other simulations carried out prove conclusively that due to the multi-paths influence, the biased bearing estimate of C-based processors is inevitable, so M-based processors must be adopted.

4. Spatial Spectrum Analysis under Sediment Parameter Uncertainty

Having established the ability of the multi-path based processor to achieve accurate bearing estimate in shallow water, we shall study the performance in greater detail. In this simulation, the spatial spectrum is analyzed under the sediment parameters uncertainty. The incident bearing angle is $\varphi = 35°$ and the array model mismatch is -10 dB. In this example, the sediment parameters uncertainty means that the sound speed and the density in sediment do not match the original simulation conditions, and are respectively assumed to be 1600 m/s and 1.5×10^3 kg/m^3. The array model mismatch is defined as

$$10\log_{10}\left(\frac{\|\delta \boldsymbol{B}\|_F^2}{\|\boldsymbol{B}_{[true]}\|_F^2}\right) \tag{38}$$

where $\|\bullet\|_F$ is the Frobenius Norm, the $\delta\boldsymbol{B}$ is the disturb of $\boldsymbol{B}$, and $\boldsymbol{B}_{[true]}$ is the actual value of $\boldsymbol{B}$.

Fig. 9 shows the spatial spectrum for M-CBF, M-SCB and M-VORB by different line types. It is obvious from the simulation figure that our proposed M-VORB significantly outperforms M-CBF and M-SCB. For example, the main-lobe is narrower and the side-lobe is lower. By this simulation, we can confirm that the performance of M-VORB is better than M-CBF and M-SCB under the sediment parameter uncertainty.

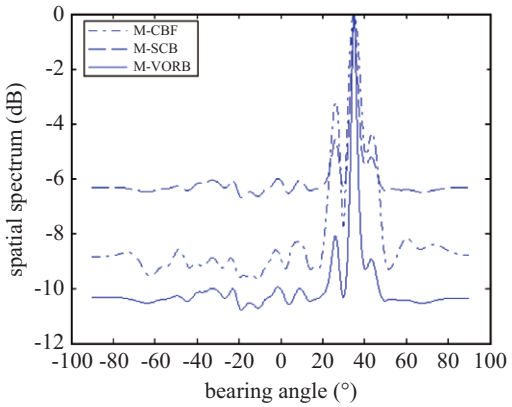

Fig. 9. The spatial spectrum under the sediment parameters uncertainty.

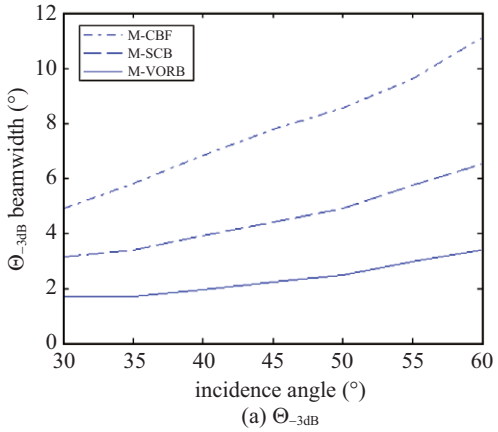

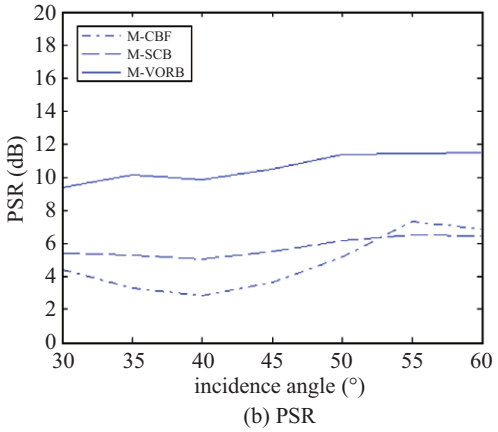

Fig. 10. Θ_{-3dB} and PSR versus incidence bearing angles under the sediment parameter uncertainty.

-3dB beamwidth (Θ_{-3dB}) and Peak to Sidelobe Ratio (PSR) are two important parameters for the analysis of the processor's performance.

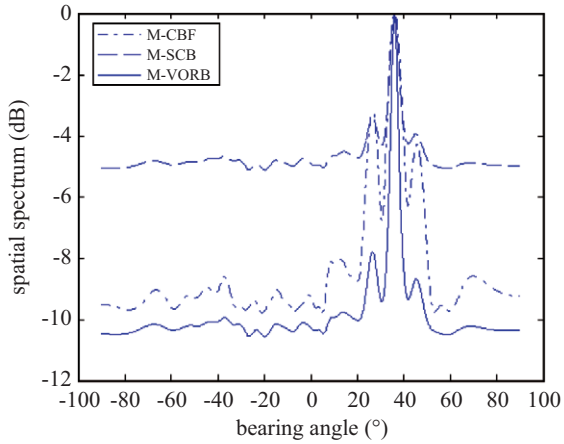

Fig. 11. The spatial spectrum under the water depth uncertainty.

Fig. 10(a) and (b) respectively show Θ_{-3dB} and PSR versus incidence bearing angles for different processors. It is shown that Θ_{-3dB} increases as the incidence bearing angle increases, and PSR varies slightly. However, as for M-VORB, the Θ_{-3dB} is narrower and the PSR is higher than other two methods at all times.

5. Spatial Spectrum Analysis under Water Depth Uncertainty

In this example, there exists a water depth uncertainty in stead of the sediment parameter uncertainty and the water depth uncertainty means that the actual water depth is 1.2 m deeper than the original simulation condition.

Fig. 11 shows the spatial spectrum and Fig. 12 indicates the Θ_{-3dB} and PSR versus incidence bearing angles. All the numerical results clearly demonstrate that M-VORB can estimate the incident bearing angle accurately with narrower main-lobe and lower side-lobe than M-CBF and M-SCB under the water depth uncertainty.

VI. CONCLUSION

In this paper, a new bearing estimation method in shallow water has been proposed, which is highly robust against the imprecise knowledge of the underwater channel parameters and the array model mismatches. It is shown that our technique makes explicit use of the multi-path nature of acoustic propagation in shallow water and the excellent performance of VORB to provide sufficient robustness improvements for bearing estimation. We have shown that the formulation of M-VORB can be transformed into the SOCP form, and then efficiently solved by SEDUMI. Computer simulations and experiments analysis have shown excellent performance of M-VORB as compared with several other conventional algorithms, such as the narrower main-lobe and lower sidelobe. SEDUMI is based on the interior-point methods whose convergence needs some time in practice, so further work about how to implement M-VORB more efficiently is required.

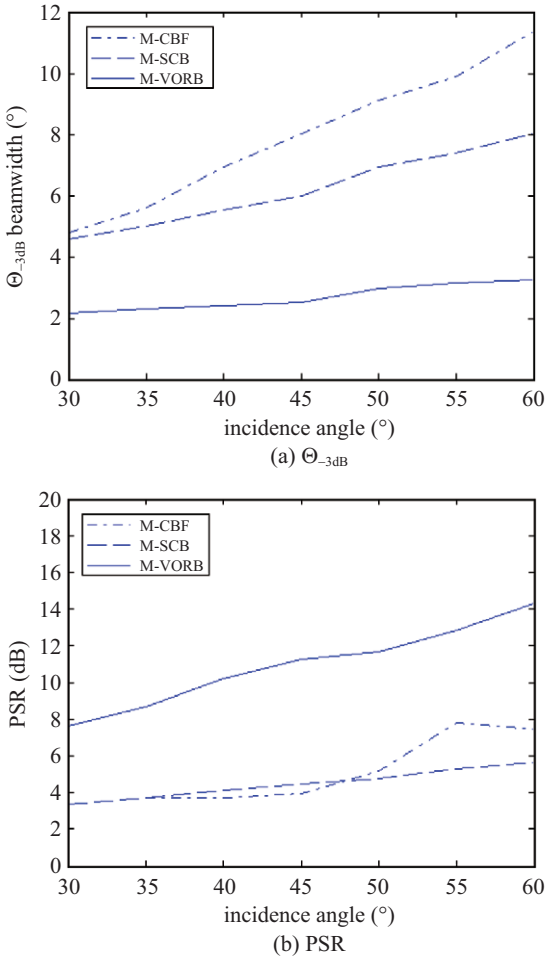

Fig. 12. Θ_{-3dB} and PSR versus incidence bearing angles under the water depth uncertainty.

ACKNOWLEDGMENTS

This work was supported by the Specialized Research Fund for the Doctoral Program of Higher Education of China (Grant No. 20122304120011), and the Natural Science Foundation of Heilongjiang Province, China (Grant No. QC2014C079), and the Scientific Research Fundation of the Education Department of Heilongjiang Province, China (Grant No. 12541657). The authors would like to thank Professor Sheng-Chun Piao of Harbin Engineering University for his helpful discussion and advice.

REFERENCES

Baggeroer, A. B., W. A. Kuperman and P. N. Mikhalevsky (1993). Overview of matched field methods in ocean acoustics. IEEE Journal of Oceanic Engineering 18(4), 401-424.

Boyd, S. and L. Vandenberghe (2006). Convex Optimization. Cambridge University Press, Oxford.

Buckingham, M. J. (1984). On the response of a towed array to the acoustic field in shallow water. IEE Proceedings, Part F: Communications, Radar and Signal Processing 131(3), 298-307.

Carey, W. M., J. F. Lynch and W. L. Siegmann (2006). Sound transmission and

spatial coherence in selected shallow-water areas: measurements and theory. Journal of Computational Acoustics 14(2), 265-298.

Chouhan, H. M. and G. V. Anand (1993). Normal mode wave-number estimation using a towed array. Journal of the Acoustical Society of America 93(4), 1807-1814.

Dosso, S. E. and M. J. Wilmut (2012). Maximum-likelihood and other processors for incoherent and coherent matched-field localization. Journal of the Acoustical Society of America 132(4), 2273-2285.

Heaney, K. D. (2011). Shallow water narrowband coherence measurements in the Florida Strait. Journal of the Acoustical Society of America 129(4), 2026-2041.

Hou, Y. S., J. G. Huang and L. J. Zhang (2008). A novel bearing estimation method for shallow water targets. Journal of Xi'an Jiaotong University 42(10), 1295-1299. (in Chinese)

Karthikeyan, C. (1986). Directional response of a towed array in shallow sea. IEE proceedings, Part F: Communications, Radar and Signal Processing 133(2), 138-145.

Krasny, L. G. and S. P. Antonyuk (1997). Wave-number estimation in an ocean waveguide. Journal of the Acoustical Society of America 102(5), 2697-2704.

Krim, H. and M. Viberg (1996). Two decades of array signal processing research: The parametric approach. IEEE Signal Processing Magazine 13, 67-94.

Lakshmipathi, S. and G. V. Anand (2004). Subspace intersection method of high-resolution bearing estimation in shallow ocean. Signal Processing 84(8), 1367-1384.

Lee, K. C., J. S. Ou and M. C. Huang (2009). Underwater acoustic localization by principal components analyses based probabilistic approach. Applied Acoustics 70(9), 1168-1174.

Li, C. M., J. C. Wu and I. T. Tang (2007). An analytic analysis of W-CDMA smart antennas beamforming using complex conjugate and DOA methods. Journal of Marine Science and Technology 15(4), 287-294.

Li, J., P. Stoica and Z. S. Wang (2003). On robust Capon beamforming and diagonal loading. IEEE Transactions on Signal Processing 51(7), 1702-1715.

Madadi, Z., G. V. Anand and A. B. Premkumar (2011). A new method for 3D localization using a hybrid array in shallow ocean with non-Gaussian noise. OCEANS 2011 IEEE, Spain, 1-7.

Markovich, G. S. and S. C. Gannot (2012). Low-complexity addition or removal of sensors/constraints in LCMV beamformers. IEEE Transactions on Signal Processing 60(3), 1205-1214.

Nagananda, K. G. and G. V. Anand (2010). Subspace intersection method of high-resolution bearing estimation in shallow ocean using acoustic vector sensors. Signal Processing 90(1), 105-118.

Naidu, P. S. (1991). On subspace method for source localization. Journal of the Acoustical Society of America 90(5), 2489-2491.

Naidu, P. S. and T. Ganesan (1995). Source localization in a partially known shallow-water channel. Journal of the Acoustical Society of America 98(5), 2554-2559.

Song, H. Y., S. C. Piao and J. P. Qin (2012a). Performance analysis of robust adaptive beamforming based on vector optimization. Chinese Journal of Electronics 40(7), 1351-1357. (in Chinese)

Song, H. Y., S. C. Piao and J. P. Qin (2012b). Robust Adaptive Beamforming Based on Vector Optimization. Acta Armamentarii 33(10), 1222-1229. (in Chinese)

Sturm, J. F. (1999). Using SeDuMi 1.02, a MATLAB toolbox for optimization over symmetric cones. Optimization Methods and Software 11(1), 625-653.

Tolstoy, A. (1993). Matched Field Processing for Underwater Acoustics, World Scientific, Singapore.

Vorobyov, S. A., A. B. Gershman and Z. Q. Luo (2003). Robust adaptive beamforming using worst-case performance optimization: a solution to the signal mismatch problem. IEEE Transactions on Signal Processing 51(2), 313-324.

Xiao, Z., W. Xu and X. Y. Gong (2009). Robust matched field processing for source localization using convex optimization. OCEANS '09 IEEE Bremen: Balancing Technology with Future Needs, Bremen, Germany, 1-5.

Xuan, L., S. F. Yan, X. C. Ma and C. H. Hou (2011). Spherical harmonics MUSIC versus conventional MUSIC. Applied Acoustics 72(9), 646-652.

Yan, S. F. and Y. L. Ma (2005). Robust supergain beamforming for circular array via second-order cone programming. Applied Acoustics 66(9), 1018-1032.

Zhang, Y. W., D. J. Sun and D. L. Zhang (2009). Robust adaptive acoustic vector sensor beamforming using automated diagonal loading. Applied Acoustics 70(8), 1029-1033.